Liu, C., Shan, Y., Wang, Q., Harris, P., Liu, Y. and Wu, L. 2023. Impacts of measured soil hydraulic conductivity on the space-time simulations of water and nitrogen cycling. *Catena.* 226, p. 107058. https://doi.org/10.1016/j.catena.2023.107058

Catena 226 (2023) 107058

Contents lists available at ScienceDirect

Catena

journal homepage: www.elsevier.com/locate/catena

Impacts of measured soil hydraulic conductivity on the space–time simulations of water and nitrogen cycling

Chuang Liu [a,b,c], Yan Shan [b,d,1], Qiuming Wang [b,d,2], Paul Harris [b], Yi Liu [c], Lianhai Wu [b,*]

[a] Key Laboratory of Nutrient Cycling Resources and Environment of Anhui, Institute of Soil and Fertilizer, Anhui Academy of Agricultural Sciences, Hefei 230001, China
[b] Rothamsted Research, North Wyke, Okehampton, Devon EX20 2SB, UK
[c] Key Laboratory of Aquatic Botany and Watershed Ecology, Wuhan Botanical Garden, Chinese Academy of Sciences, Wuhan 430074, China
[d] College of Resources and Environment, Northwest A & F University, Yangling 712100, China

ARTICLE INFO

Keywords:
SPACSYS
K_{sat}
Process-based modelling
Soil nutrients
Grid-to-grid

ABSTRACT

In agriculture, variations in soil nutrients and water are driven by soil properties, topography and agronomic practice that typically interact and change over space and time. Agroecosystem models need to capture these sources in variation, where this study's first objective was to assess the potential of using measured saturated soil hydraulic conductivity (k_{sat}) to improve the simulation accuracy of water and soil mineral nitrogen content from the SPACSYS model for a lowland UK grazed field (6.34 ha). As a second objective, SPACSYS was run at the field level and at the within-field level to provide a further comparison of simulation accuracy. For model calibration, k_{sat} was measured at 27 points at 0–10, 10–20 and 20–30 cm soil depths on a 50 × 50 m grid. For model validation, moisture and mineral nitrogen content in the same three soil layers, at 10 adjacent points on a 25 × 25 m grid, were measured monthly from May 2018 to April 2019, together with in situ field level water flux measurement. Measured k_{sat} coupled with the within-field setting allowed a novel spatial investigation of SPACSYS performance. Measured k_{sat} (as opposed to unmeasured, default values) was found to improve water flux simulation, but only slightly so, which was considered in part due to a high positive skew in the measured k_{sat} coupled with no clear spatial structure. Field level and within-field specifications simulated soil moisture with equal accuracy, while simulation accuracy of soil ammonium and nitrate improved via the within-field setting; for water flux simulation, the field level setting should be preferred. Results provide further evidence for when a field level setting should be preferred to a within-field setting and vice-versa.

1. Introduction

In agriculture, the spatiotemporal variation of soil nutrients and water is influenced by interacting factors such as soil properties, terrain characteristics and agronomic practice (Mohanty et al., 2000). The water potential gradient drives water fluxes, and thus affects soil nutrient cycling, and plant growth and development (Alletto and Coquet, 2009; Herbst et al., 2021; Kreiselmeier et al., 2020). Similarly, biological dynamics in the land management system can induce fluctuations of soil water content (Liu et al., 2018). Because of the complexity of the interactions between soil water, nutrient, plant and hydrology, understanding and accurately quantifying processes for water redistribution and nutrient cycling in the soil, plant and atmospheric domains is an on-going challenge. Furthermore, characterization of these processes at an appropriate spatial and temporal scale is essential to accurately quantify the effects on ecosystem management (Centeno et al., 2020; Rathjens and Oppelt, 2012; Rienzner and Gandolfi, 2014). However, difficulties arise in measuring such dynamic processes, as measurement, particularly at the required spatial resolution, is often costly and time consuming (West et al., 2010; Zhang et al., 2014; 2015). As an alternative, process-based models can be applied that have a spatial component, where a 'grid-to-grid' methodology is employed that divides an object area into a finite number of cells to form a grid structure on which all of the operations are implemented individually (Rathjens et al., 2015; Zhang et al., 2014; 2017).

The SPACSYS (Soil-Plant-Atmosphere Continuum SYStem) model

* Corresponding author.
E-mail address: lianhai.wu@rothamsted.ac.uk (L. Wu).
[1] current address: Institute of sericulture, Shandong Academy of Agricultural Sciences, Yantai, 264001, Shandong, China.
[2] current address: College of Urban and Environmental Sciences and MOE Laboratory for Earth Surface Processes, Peking University, China.

https://doi.org/10.1016/j.catena.2023.107058
Received 29 July 2022; Received in revised form 29 December 2022; Accepted 1 March 2023
Available online 9 March 2023

(Wu et al., 2007) has been widely adopted to simulate plant growth, soil carbon (C), nitrogen (N) and phosphorus (P) cycling, water redistribution at the field scale - either for arable land (Bingham and Wu, 2011; Liu et al., 2020; Wu et al., 2019; Zhang et al., 2016) or for grassland (Li et al., 2017; Wu et al., 2015; 2016), with a daily time step. SPACSYS has been recently spatially-adapted to capture within-field processes with the 'grid-to-grid' approach where the field was overlaid with a representative grid to consider lateral nutrient and water exchange between adjacent grid cells, and where it was shown to improve simulation accuracy over the default field scale ('single-point') version (Liu et al., 2018). However, in Liu et al., (2018), the soil hydro-physical properties were naively taken at the field level only, i.e., treated uniformly across the study field with default, unmeasured information.

Soil hydro-physical properties are essential in understanding key processes of the hydrological cycle and in turn, can ensure efficient management of water resources (Beskow et al., 2016; Lim et al., 2020; Wösten et al., 2001). Saturated soil hydraulic conductivity (k_{sat}) is one such measure (Alletto and Coquet, 2009; Li et al., 2017; Nikodem et al., 2021). However spatially, k_{sat} typically exhibits high variability (Baiamonte et al., 2017; She et al., 2017), driven by variation in soil texture and pore space geometry, topography and geology (Baiamonte et al., 2017; Centeno et al., 2020; Ming et al., 2020; Papanicolaou et al., 2015), which in turn, influences land–atmosphere interaction, plant growth, surface runoff and nutrient movement.

Thus, directly building upon the previous implementation of the 'grid-to-grid' method with SPACSYS (Liu et al., 2018), this study focused on simulations for soil moisture, water fluxes and soil mineral N at the same grid resolution of 25 × 25 m but now across a much larger grazed field of the same research farm in southwest England, UK. This new study was also for a different grass variety, had a richer model validation dataset with different processes, and had measured k_{sat} (rather than a default value) for model calibration. In summary, the key objective was to simulate nutrient cycling more accurately than that found using defaults at field level by considering: 1) within-field measurements of k_{sat} and 2) within-field water pathways via the 'grid-to-grid' model formulation.

2. Materials and methods

2.1. The SPACSYS model

Detailed descriptions of SPACSYS are given elsewhere (Wu, 2019; Wu et al., 2007). Briefly, the model includes a plant growth and development component, N, C and P cycling components, a soil water component, together with a heat transfer component. Core processes concerning a plant are plant development, assimilation, respiration, nutrient and water uptake, and the partition of photosynthate and nutrients, plus N fixation for legume plants, and root growth and development. N cycling coupled with C cycling covers the transformation processes for organic matter and inorganic N including mineralization, nitrification and denitrification. The Richards equation for water potential and the Fourier's equation for temperature are used to simulate water and heat fluxes. In this study, we only focus on water redistribution and N cycling.

Commonly, SPACSYS is applied at the field scale (single-point setting) where processes are assumed to be uniformly distributed across the whole field, and where the means of observed data represent the field. To account for spatial variation of soil water and nutrients within a field, SPACSYS provides a sub-field (grid-to-grid or 'multiple-point') setting that divides a field into grid cells (or square pixels) with flexible length that consider the topographical inter-connections of the field's water flow pathways. At each time step, the model runs simulations that traverse all grid cells starting from those that have no upstream linkage. Water and nutrient flows out of a grid cell via runoff and drainage are passed to its recipient grid cell as inputs before the simulation for the grid cell starts. Apart from exchanges in water and nutrients with the linked grid cells, each grid cell is treated as an independent entity with assigned soil physical and chemical properties, including k_{sat} and management. Such detailed within-field characterisation has the potential to improve model performance over the default (single-point) version provided data are available at the grid cell resolution.

2.2. Study site

The study field is located on the North Wyke Farm Platform (NWFP) which is a farm-scale experiment situated at the North Wyke campus of Rothamsted Research in southwest England (50°46′12″N, 3°54′05″W). The soils belong predominantly to two similar series: Hallsworth (Dystric Gleysol) and Halstow (Gleyic Cambisol), which comprise a slightly stony clay loam topsoil (*ca.* 36% clay) that overlies a mottled stony clay (*ca.* 60% clay), derived from underlying Carboniferous culm rocks (Harrod and Hogan, 2008). From 1982 to 2019, the average annual precipitation at North Wyke was 1031 mm (minimum and maximum values of 705 and 1361 mm, respectively) together with average minimum and maximum daily temperatures of 6.8 and 13.5 °C, respectively. The average annual potential evapotranspiration from 2015 to 2019 was 575 mm (Stanley et al., 2021).

The 63 ha site was established in 2010 and consists of 15 hydrologically isolated sub-catchments across three 21 ha small farms (farmlets) with five sub-catchments in each (Orr et al., 2016). The platform routinely monitors livestock and silage performance together with records of farm management events. These data are coupled with primary collections for weather elements, soil moisture, water flux and chemistry, and greenhouse gases. To calibrate and validate SPACSYS, measurements for soil water and soil mineral N content were conducted in Great Field of the re-seeded monoculture farmlet in 2018/19 (re-seeded from permanent pasture in 2013). This sub-catchment (6.34 ha) slopes downwards from an east to west direction, to a water flume in its west corner, where water flux from the sub-catchment is measured at a 15 min interval. For this study, the sub-catchment was virtually divided into 107 grid cells resulting from a 25 × 25 m grid where grid cell linkages were based on water potential moving direction, so the grid-to-grid approach could be applied. It was assumed that each 25 × 25 m grid cell has eight possible drainage flow directions and where each grid cell only has up to one downstream grid cell. This resulted in eleven hydrological flow lines as depicted in Fig. 1.

2.3. Model calibration: Soil hydraulic conductivity measurements

For model calibration, k_{sat} was measured by the falling head technique. Twenty-seven points at 0–10, 10–20 and 20–30 cm soil depths were measured on a 50 × 50 m grid across the whole of Great Field over the period between March to July 2019 (Fig. 1). Undisturbed soil samples were taken using a 250 ml volume steel cylinder with 8 cm inner diameter and 5 cm height (cores were taken in the middle of each soil layer). The k_{sat} measurement was performed using a KSAT® device (METER Group AG, Munich, Germany). Measured k_{sat} for the three soil depths are shown in Fig. 2. For all depths, the k_{sat} measurements were highly positively skewed and with no clear spatial structure. At each of the three soil depths, the measured k_{sat} data were subsequently interpolated to the 25 × 25 m simulation grids (Fig. 1) using inverse distance weighting (IDW) (via functionality in ArcGIS version 10.2, www.esri.com). Thus, for the grid-to-grid method, k_{sat} datasets are found for each soil layer, each consisting of 107 interpolated k_{sat} values covering all 25 m grid cells.

2.4. Model validation: Soil moisture and nitrogen measurements

Soil water (soil weight fraction), soil ammonium (NH_4^+-N) and nitrate (NO_3^--N) contents at depths of 0–10, 10–20 and 20–30 cm at ten grid cell locations (25 × 25 m grid, highlighted by red grid cells in Fig. 1) along three downstream lines (highlighted by green lines in Fig. 1) were

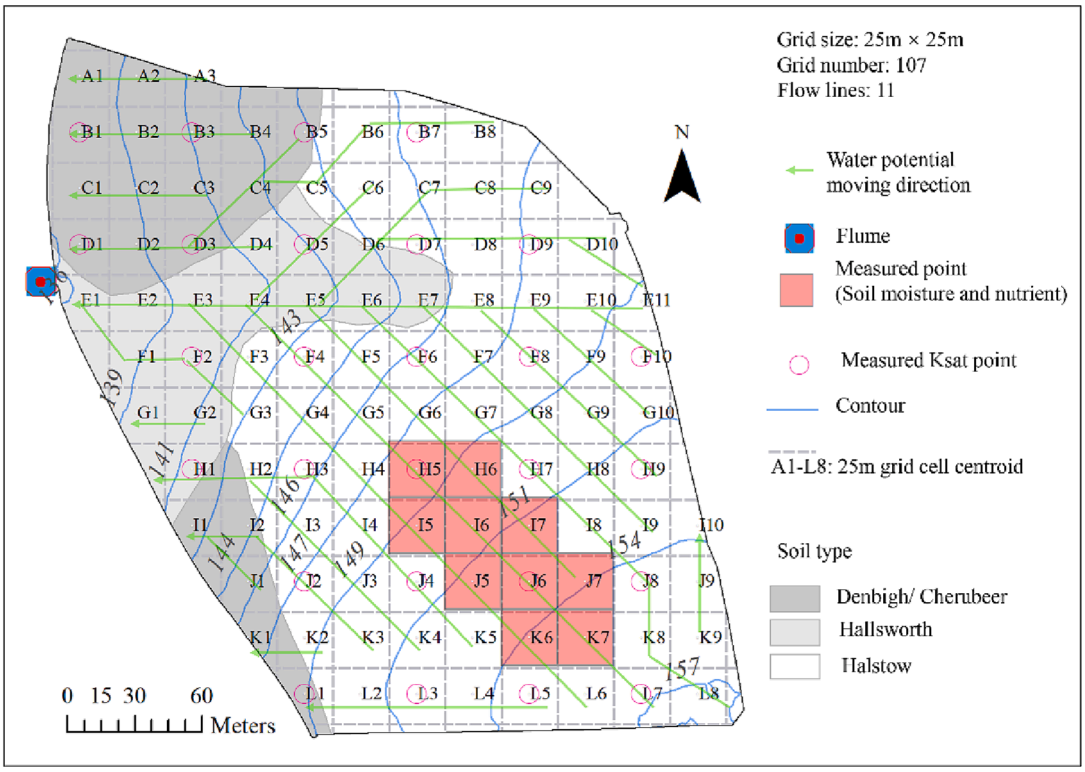

Fig. 1. Elevation, soil type and water runoff collection point (flume) in Great Field with 27 measurement points for k_{sat} (on a 50 × 50 m grid); 10 measurement points for soil moisture, ammonium and nitrate (all on a 25 × 25 m grid); and 107 grid-cell SPACSYS simulation points (also on the 25 × 25 m grid) with grid cells labelled by row moving in a southward manner (A1 to L8). Water potential moving direction shown by green lines, three of which traverse the soil moisture and nutrient measurements. (For interpretation of the references to colour in this figure legend, the reader is referred to the web version of this article.)

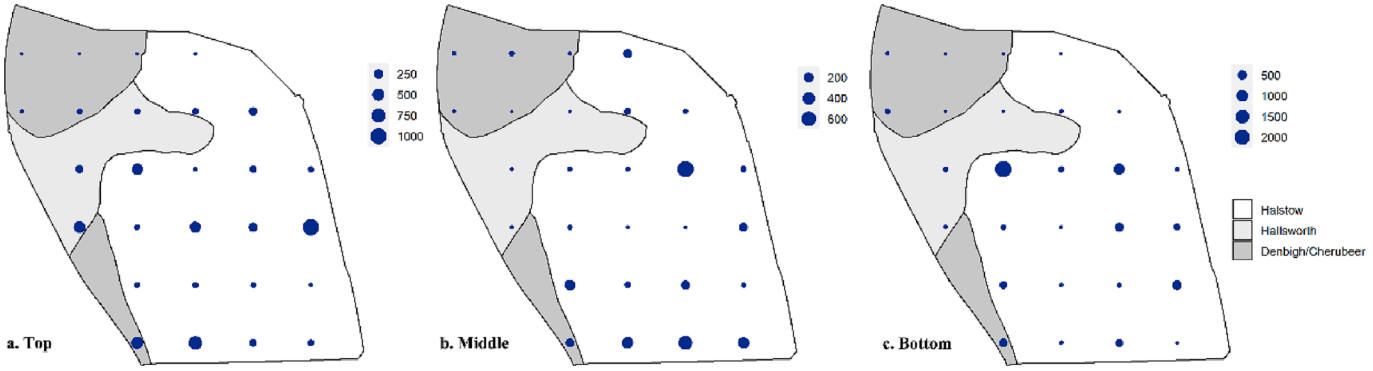

Fig. 2. Measured soil saturated hydraulic conductivity (k_{sat}, cm d^{-1}) sampled on a 50 m grid at (a) 0–10 cm, (b) 10–20 cm (b) and (c) 20–30 cm soil depths in Great Field. Maps are shown with the soil series.

measured monthly from May 2018 to April 2019. For the soil measurements, roughly 100 g of soil from each soil layer was taken and then sieved over a 2 mm mesh to remove roots and stones. A quarter of the sample was put into a wide-mouth 500 ml plastic bottle and 50 ml KCL extracts were added. The sealed bottle was then shaken on a reciprocating shaker for 1 h at a nominal 150 S per minute. The filtered solution from the bottle was used to measure N contents. The rest of the sampled soil was weighted and dried for over 8 h at 105 °C, and then weighed again to calculate soil moisture.

2.5. Simulation design and SPACSYS parameterisation

For calibrating SPACSYS, input parameters on soil physical properties of the three soil types in Great Field (Fig. 1), including the default k_{sat} value, were estimated by the pedo-transfer function based on soil texture and soil organic matter content (Cosby et al., 1984). For validating SPACSYS, measured soil moisture, NH_4^+-N and NO_3^--N contents at the ten grid cells between May 2018 and April 2019 were used, together with water flux measurements from January 2011 to December 2019. Four model simulation scenarios were defined as follows:

1) a single simulation for the field (single-point) with a single k_{sat} value in a soil layer taken as the mean of the estimated k_{sat} values in the layer for the three soil types. This is unmeasured k_{sat} and referred to as the default k_{sat} value thereafter;
2) a single simulation using the single-point method with a single k_{sat} value in a soil layer taken as the mean of the measured k_{sat} in the layer;
3) multiple simulations (at 107 grid cells) using the grid-to-grid method with the default k_{sat} value as used in scenario 1 for all grid cells;

4) multiple simulations using the grid-to-grid method with k_{sat} values for each of the 107 grid cells. For brevity, this scenario was still referred to as using the measured k_{sat} values given that 27 of the 107 k_{sat} interpolations were still the same as those measured, as IDW was used in an exact interpolator form (i.e., IDW honoured existing measurements).

Scenarios 1 and 3 relate to the typical situation when no measurements of k_{sat} exist. When the simulations using the single-point method are compared with the measured data, it was assumed that mean soil moisture, and NH_4^+-N and NO_3^--N contents measured over the ten grid cells at a time are representative of the entire field, at any given time. For the grid-to-grid method, simulated water fluxes from each flow line are summed to represent the water fluxes from the field. To compare with the single measured water flow at the flume, at each time step, soil water and soil nutrients out of a grid cell through surface runoff and drainage flow are passed to its recipient grid cell as inputs. All other aspects of model parameterisation and initial conditions were the same as that used in previous SPACSYS studies on the NWFP (Li et al., 2017; Liu et al., 2018).

2.6. Statistical analysis for model performance

The following statistical indices were used to assess SPACSYS performance (Smith et al., 1997): (a) the root mean squared error (RMSE) that reflects the average size of the error between measured and simulated data (for an accurate simulation this should tend to zero); (b) modelling efficiency (EF, the closer to unity, the better) that quantifies the accuracy and confidence of the simulation; (c) the coefficient of determination (CD, the closer to unity, the better) that describes the goodness of fit between measured and simulated data; (d) the correlation coefficient (r) between measured and simulated data which should tend to unity; (e) the relative error (RE); and (f) the mean error (ME). Here RE and ME are used to assess bias (tendencies for over- and under-prediction) in the simulations as they reflect differences between measured and simulated data.

3. Results

3.1. Soil moisture

The spatiotemporal variation in the measured soil moisture in the three soil layers is shown in Fig. 3. The data exhibited moderate levels of positive skew at all three depths. As expected, soil moisture varied across months and by depth. In summer (June–August), the soil was dry in each measured layer. From November to May, soil moisture in the topsoil was relatively high, while throughout the year, the bottom layer showed persistent lower water content. There were no apparent spatial patterns along the three downstream lines that traverse the 10 measured grid cells.

Comparisons between simulated and measured soil moisture are shown in Fig. 4 and the corresponding performance indices are presented in Table 1. Temporal trends of the measured data were broadly reproduced by the simulations for all four scenarios, especially when the soil was getting drier. However, large discrepancies between measured and simulated soil moisture occurred in winter, commonly the wettest period. Visually, the grid-to-grid simulations appear to better capture the fluctuations of measured soil moisture at each soil depth compared with the single-point simulation although the peaks of the measured soil moisture were somewhat under-predicted by the simulations.

The performance indices, however, suggested little difference in soil moisture simulations between single-point and grid-to-grid modes and regardless of whether default k_{sat} (scenarios 1 and 3) or measured k_{sat} (scenarios 2 and 4) were used. On average for each soil depth, the single-point simulations performed similarly to that from grid cells H6, J5 and K7 (Fig. 1) in the grid-to-grid simulations, where these cells were closest to the locations in the last third grid cell of each water flux direction (Fig. 1). SPACSYS tended to under-predict soil moisture for all four simulation scenarios across all periods and depths, as RE and ME were always positive, where scenario 1 consistently resulted in the smallest prediction bias. As all r values > 0.73, simulation under any scenario showed reasonably accurate prediction in soil moisture, with the weakest performance in the lower layer (the smallest r coupled with CD values > 4).

3.2. Soil ammonium content

Spatiotemporal variation in soil NH_4^+-N content across the ten sampled grid cells at different depths in the logarithmic form are shown in Fig. 5. Relatively high NH_4^+-N content was often found in the upper grid cells (K6, K7) in each soil layer. Relatively high NH_4^+-N was also found in June, July and March, especially in the top layer, likely coinciding with recent fertilizations (see Fig. 6, below). Overall, there was no clear change in soil NH_4^+-N along the downstream water flux direction lines. The raw NH_4^+-N data ranged from a minimum of 0.01 mg N kg^{-1} soil in October and November 2018 to a maximum of 129.5 mg N kg^{-1} soil in March 2019 (Fig. A1).

Comparisons between simulated and measured soil NH_4^+-N are shown in Fig. 6 and the corresponding performance indices are presented in Table 2. As with soil moisture, the temporal trends in measured

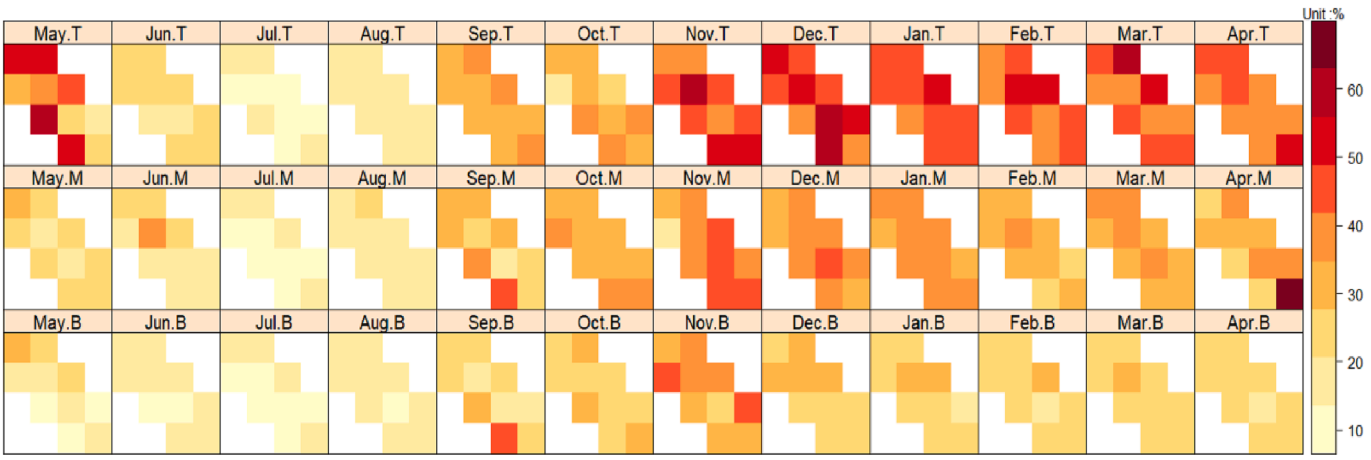

Fig. 3. Spatiotemporal variation in soil moisture at depths of 0–10 cm (top row, 'T'), 10–20 cm (middle row, 'M') and 20–30 cm (bottom row, 'B') across the ten grid cells highlighted in Fig. 1 (labelled H5, H6, I5, I6, I7, J5, J6, J7, K6 and K7). Data measured monthly from May 2018 to April 2019.

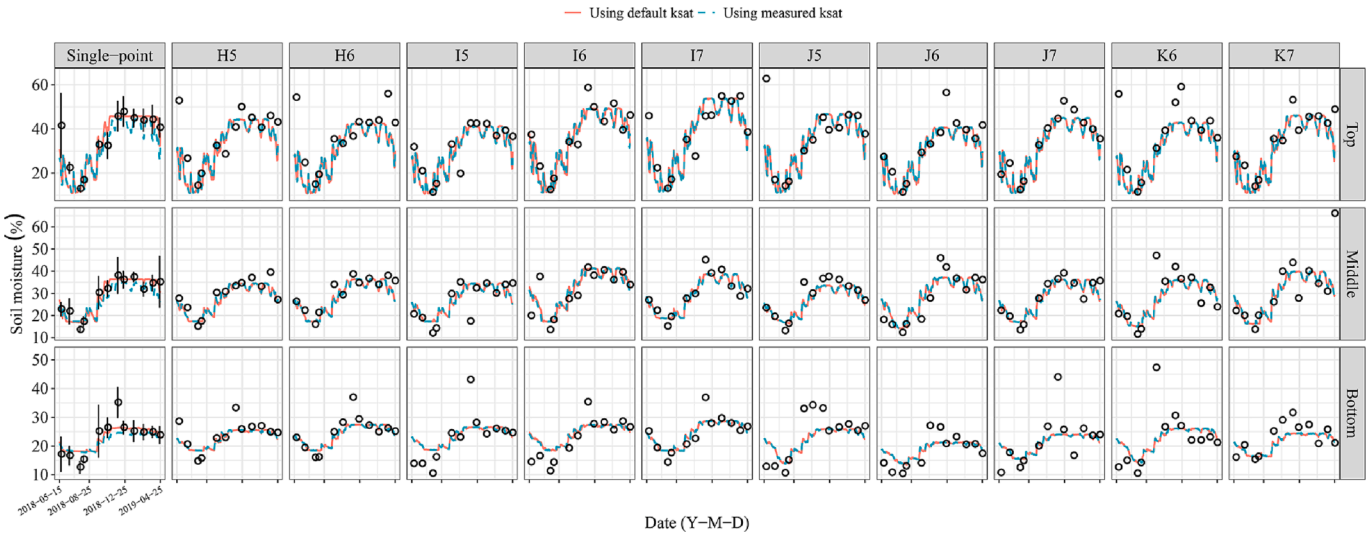

Fig. 4. Temporal comparison of measured (points) and simulated (lines) soil moisture for the single-point simulation (scenarios 1 and 2 with default and measured k_{sat}, respectively) and grid-to-grid simulations (scenarios 3 and 4 with default and measured k_{sat}, respectively) at depths of 0–10 cm (Top), 10–20 cm (Middle), 20–30 cm (Bottom) from May 2018 to April 2019. The x-axes are the same for all the grids as the single-point. Scenarios with the default k_{sat} are given with a red unbroken line, while those with measured k_{sat} are given with a blue dashed line. Grid-to-grid simulations are given at each of the ten grid cells highlighted in Fig. 1 (labelled H5, H6, I5, I6, I7, J5, J6, J7, K6 and K7). (For interpretation of the references to colour in this figure legend, the reader is referred to the web version of this article.)

Table 1
Statistical performance indices for soil moisture at soil depths of 0–10 (Top), 10–20 (Middle) and 20–30 cm (Bottom) for the single-point and grid-to-grid simulation scenarios with default and measured k_{sat}.

Soil layer	Index	Single-point (n = 12)		Grid-to-grid (n = 120)	
		Scenario 1 default k_{sat}	Scenario 2 measured k_{sat}	Scenario 3 default k_{sat}	Scenario 4 measured k_{sat}
Top	RMSE	0.25	0.30	0.27	0.27
	EF	0.54	0.35	0.46	0.46
	CD	1.03	1.29	1.20	1.20
	r	0.78	0.75	0.78	0.78
	ME	0.02	0.06	0.05	0.05
	RE	6.95	16.03	13.59	13.36
Middle	RMSE	0.20	0.23	0.20	0.20
	EF	0.62	0.50	0.61	0.61
	CD	1.51	2.22	1.81	1.81
	r	0.79	0.77	0.79	0.79
	ME	0.00	0.03	0.01	0.01
	RE	0.65	9.23	4.04	3.94
Bottom	RMSE	0.23	0.26	0.23	0.23
	EF	0.46	0.35	0.47	0.47
	CD	5.10	8.91	4.19	4.18
	r	0.74	0.73	0.73	0.73
	ME	0.00	0.01	0.00	0.00
	RE	0.07	5.17	1.62	1.59

Note: RMSE: the root mean squared error; EF: modelling efficiency; CD: the coefficient of determination; *r*: the correlation coefficient; RE: the relative error and ME: the mean error.

soil NH_4^+-N were broadly reproduced with the simulations, often picking up key step changes over time, especially in the topsoil layer. Performance indices clearly indicate the grid-to-grid simulations to better represent the measured soil NH_4^+-N than the single-point simulations, but in the topsoil only (for example, *r* values of 0.74 to 0.76 for grid-to-grid rather than 0.23 to 0.28 for single point). However, simulated NH_4^+-N in the grid cells of the middle downstream water flux direction line (H5, I6 and J6 from Fig. 1) poorly matched the measured values (Fig. 6). On viewing the performance indices, all simulation scenarios performed poorly at the middle and bottom soil layers as highlighted with negative *r* values, but where grid-to-grid simulations reduced bias over single-point simulations (as they lowered ME and RE). The use of measured (scenarios 2 and 4) rather than default k_{sat} values (scenarios 1 and 3) did not provide an improvement in the simulations for any scenario.

3.3. Soil nitrate content

Spatiotemporal variation in soil NO_3^--N content over the ten sample grid cells for the three depths in the logarithmic form are shown in Fig. 7. Clearly, soil NO_3^--N was relatively high in the topsoil throughout the year, but where differences were weaker in September, October and November (as for these months, soil NO_3^--N was broadly similar through the layers). The raw NO_3^--N data ranged from a minimum of 0.05 mg N kg^{-1} soil in May and June 2018 to a maximum of 106.9 mg N kg^{-1} soil in March 2019 (Fig. A2).

Comparisons between simulated and measured soil NO_3^--N are shown in Fig. 8 and the corresponding performance indices are presented in Table 3. Again, the measured temporal trends were broadly reproduced with the simulations. It appears that grid-to-grid simulations capture seasonal fluctuations much better than those from the single-point method, although the peak between September and October 2018 was only captured with the single-point method.

Similar to soil NH_4^+-N, the performance indices indicate the grid-to-grid simulations better represent measured soil NO_3^--N than the single-point simulations, especially in the topsoil layer (for example, *r* values of 0.81 to 0.84 for grid-to-grid rather than 0.22 to 0.26 for the single point). For the middle and bottom soil layers, there was little to choose between any of the four modelling scenarios with respect to simulation accuracy. Again, the use of measured rather than default k_{sat} values did not improve simulation accuracy.

3.4. Water fluxes

Simulated water fluxes were visually compared with measured fluxes over the nine-year period between 2011 and 2019, as shown in Fig. 9. As indicted by the performance indices (Table 4), the single-point simulation using the measured k_{sat} value was the most accurate (lowest RMSE and strongest *r* values) with relatively small bias (smallest RE and ME values), then that using the default k_{sat} value. Unlike the results above, the grid-to-grid simulations performed poorly in comparison to the single-point simulations.

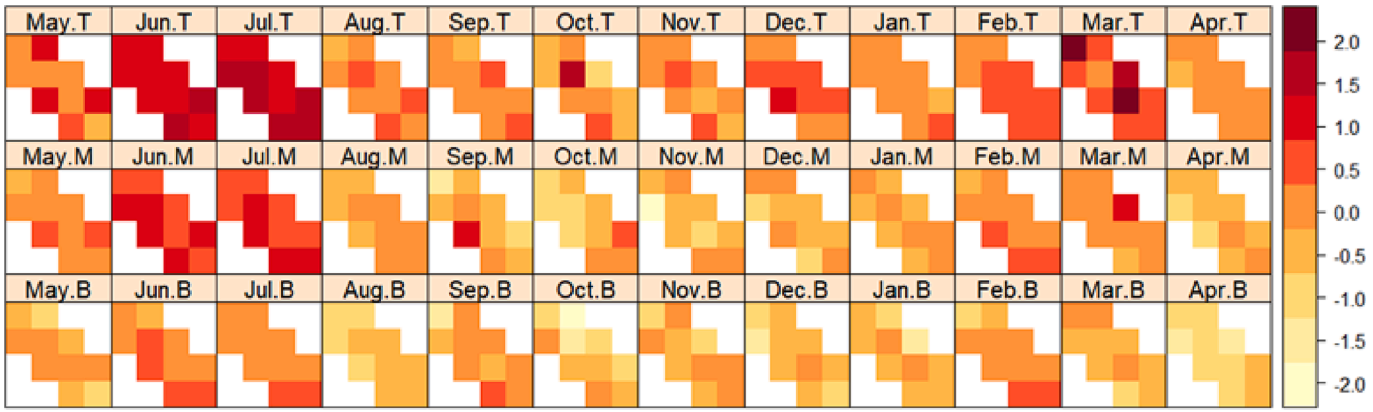

Fig. 5. Spatiotemporal variations in soil NH_4^+-N content (mg N kg^{-1} soil) at 0–10 cm (top row, 'T'), 10–20 cm (middle row, 'M') and 20–30 cm (bottom row, 'B') across the ten grid cells highlighted in Fig. 1 (labelled H5, H6, I5, I6, I7, J5, J6, J7, K6 and K7). Data measured monthly from May 2018 to April 2019 and presented in logarithmic (base 10) form.

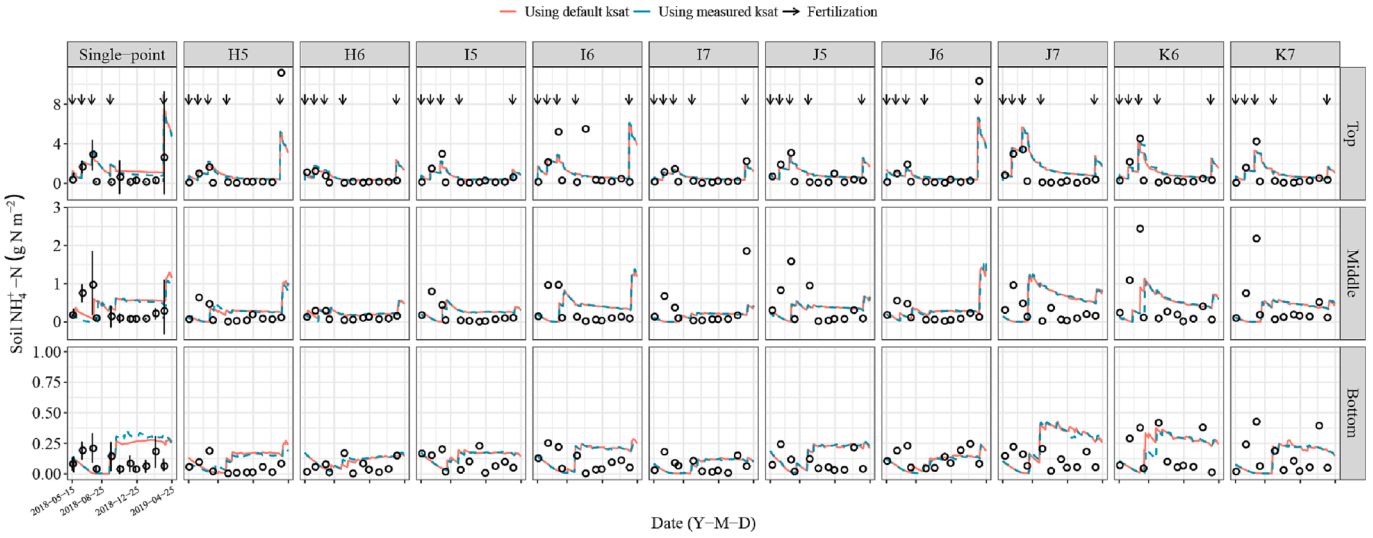

Fig. 6. Temporal comparison of measured (points) and simulated (lines) soil NH_4^+-N content for the single-point simulations (scenarios 1 and 2 with default and measured k_{sat}, respectively) and grid-to-grid simulations (scenarios 3 and 4 with default and measured k_{sat}, respectively) at depths of 0–10 cm (Top), 10–20 cm (Middle), 20–30 cm (Bottom) from May 2018 to April 2019. The x-axes are the same for all the grids as the single-point. Scenarios 1 and 3 are given with a red unbroken line, while the others are given with a blue dashed line. Grid-to-grid simulations are given at each of the ten grid cells highlighted in Fig. 1 (labelled H5, H6, I5, I6, I7, J5, J6, J7, K6 and K7). Times of fertilization are also shown. (For interpretation of the references to colour in this figure legend, the reader is referred to the web version of this article.)

4. Discussion

4.1. Characteristics of measured k_{sat}

Clearly, k_{sat} is a key input parameter for any process-based hydrological model. However, this study's largely null results tend to reflect its highly variable nature with k_{sat} values changing markedly over space. High positively skewed distributions of measured k_{sat} had no clear spatial structure, where their empirical variograms tended to random variation (not shown) for each soil layer. This is in agreement with existing work regardless of the measurement methodology, geographical location, land use, soil type and scale (Centeno et al., 2020; Papanicolaou et al., 2015; She et al., 2017). As a soil hydro-physical variable, k_{sat} typically responds to changes in topography (e.g., elevation and slope) and small-scale changes in soil macroporosity (Centeno et al., 2020; She et al., 2017), which is reflected in its highly localised nature. Given such localised properties of k_{sat}, it was unsurprising that only for the simulation of water flux, a field scale process, did the use of measured k_{sat} hold any promise (scenario 2).

Further, for scenario 4 which was never considered as the best scenario, the IDW interpolation of k_{sat} to the 25 m grid would have been somewhat compromised by the underlying localised properties of measured k_{sat} in the first place. In hindsight, measuring k_{sat}, at the same scale of the simulations (i.e., the 25 m grid) may have been a better approach, where uncertainties due to the IDW interpolation would not arise. In addition, using only three depths could have been limiting given the differences observed across depths in Fig. 2; and this study did not consider temporal changes in measured k_{sat} (i.e., k_{sat} was assumed time invariant).

Thus, characteristics of the k_{sat} distributions are dictated by the sample resolution (in space, time and depth), where this study's 50 m grid was likely to be too coarse to robustly detect true spatial structure in k_{sat}. The ideal spatial resolution is likely to be a trade-off between inherent practical considerations in k_{sat} measurement and the scale at which the core components of the water cycle are expected to operate at. Difficulties then arise, in that different components can operate at their own spatial scale, and / or operate at a range of spatial scales (i.e., multi-scale in nature).

Table 2
Statistical performance indices for soil NH_4^+-N content at soil depths of 0–10 (Top), 10 –20 (Middle) and 20–30 cm (Bottom) for the single-point and grid-to-grid simulation scenarios with default and measured k_{sat}.

Soil layer	Index	Single-point (n = 12)		Grid-to-grid (n = 120)	
		Scenario 1 default k_{sat}	Scenario 2 measured k_{sat}	Scenario 3 default k_{sat}	Scenario 4 measured k_{sat}
Top	RMSE	2.17	2.22	1.42	1.44
	EF	−0.10	−0.15	0.53	0.51
	CD	6.24	3.82	2.45	2.38
	r	0.28	0.23	0.76	0.74
	ME	−0.71	−0.60	−0.30	−0.31
	RE	−85.16	−71.64	−35.64	−36.72
Middle	RMSE	2.08	2.10	1.93	1.92
	EF	−0.79	−0.83	−0.55	−0.53
	CD	6.25	3.37	4.55	4.80
	r	−0.58	−0.45	−0.35	−0.35
	ME	−0.17	−0.08	−0.01	0.00
	RE	−63.80	−31.25	−4.40	−1.45
Bottom	RMSE	1.70	1.93	1.44	1.44
	EF	−2.31	−3.29	−1.40	−1.39
	CD	0.86	0.65	0.95	0.94
	r	−0.25	−0.28	−0.05	−0.05
	ME	−0.08	−0.10	−0.05	−0.05
	RE	−73.50	−95.85	−45.82	−44.44

Note: RMSE: the root mean squared error; EF: modelling efficiency; CD: the coefficient of determination; *r*: the correlation coefficient; RE: the relative error and ME: the mean error.

For this study, the 25 m and 50 m grids were simply chosen to match the previous (unrelated soil) study at these resolutions (Peukert et al., 2016) and available resources for sampling. However, the resources (costs and labour) required for sampling at a higher resolution may not have provided sufficient increase in model accuracy, for it to be worthwhile. Further, sampling at a finer resolution would not guarantee that the required spatial structure is adequately captured. It may be that k_{sat} is always effectively a random process, as to detect usable spatial structure would be too costly. In this respect, if it is taken as impractical to measure k_{sat}, the pedo-transfer function used for the default k_{sat} value, appears to provide a robust k_{sat} estimate. However, this function is highly site dependent, and as such, alternatives to estimate k_{sat} could be trialled (e.g., hierarchical functions for different soils (Schaap et al., 2001)).

4.2. Characteristics of measured soil water and N contents

The measured spatio-temporal soil moisture and soil mineral N at the three soil layers all exhibited moderate to high levels of positive skew (and were thus presented in logarithmic form for soil mineral N in Figs. 5 and 7). Distributions of soil moisture largely behaved as expected, they varied across months and by depth, with low moisture values in the summer months and at the lower depth throughout the year. These relatively interpretable characteristics were carried forward to relatively accurate SPACSYS simulations of soil moisture for all four scenarios. Distributions of soil N were more challenging with no clear trends. These more challenging characteristics (including the strong levels of skew) in the measured data were similarly carried forward to the SPACSYS simulations, but where now the simulation accuracy was often much poorer in relation to that found for soil moisture, especially at the lower soil depths (Fig. 4).

Water movement and soil water content can affect the pathways of soil NH_4^+-N and NO_3^--N. A high surface water flux and quick redistribution downward could accelerate the movement of mineral N, especially NO_3^--N in soil, and speed up N losses (Dou et al., 2022; Song et al., 2022; Whitson, 2020). In our study, the vertical distribution of soil NO_3^--N and NH_4^+-N contents decreased with soil depth (Figs. 6 and 8), which follows the distribution of soil water content (Fig. 4). However, there is no spatial pattern with a water flux direction, which might be caused by heterogeneity in grass growth, grazing, excreta deposition and fertiliser spreading. Additionally, the measured soil moisture at some locations in time were higher than the estimated porosity. Such high measurements may be in error, as they did not correspond to heavy or persistent rainfall before the measurement dates or readings from an in situ soil moisture sensor located in the centre of the study field (grid cell G5 in Fig. 1).

4.3. SPACSYS model performance

Taking all four scenarios as one, SPACSYS performed reasonably and accurately for simulating soil moisture and water flux, but not so well for simulating soil N. For soil N, the grid-to-grid method provided clear improvements in simulation accuracy, especially for the top layer. Results complement and extend those of Liu et al. (2018), who focused on water flux, soil moisture, N_2O emissions and biomass in a different and smaller field of the NWFP. Liu et al. showed that the single-point method is adequate for accurate water flux and soil moisture simulations, while the grid-to-grid formulation was considered of value in terms of accurate grass biomass simulation. This study also complements that of Liu et al. (2018), in the evaluation of k_{sat} measurements for model calibration, where a still valid and reportable, null outcome has resulted.

Inevitably, discrepancies between simulated and measured values exist, which might in part be due to a likely spatial heterogeneity of the canopy as a result of uneven grazing and also root systems that affect water uptake and infiltration, which in turn impact water redistribution (Logsdon, 2013). Management simplifications used in the model could also cause discrepancies. For example, it was assumed that animals

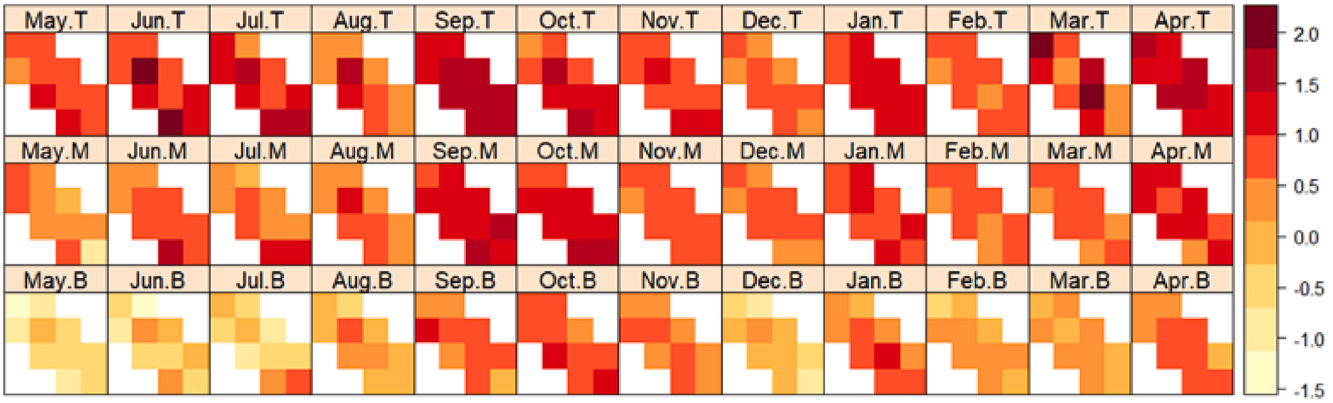

Fig. 7. Spatiotemporal variations in soil NO_3^--N content (mg N kg^{-1}) at 0–10 cm (top row, 'T'), 10–20 cm (middle row, 'M') and 20–30 cm (bottom row, 'B') across the ten grid cells highlighted in Fig. 1 (labelled H5, H6, I5, I6, I7, J5, J6, J7, K6 and K7). Data measured monthly from May 2018 to April 2019 and presented in logarithmic (base 10) form.

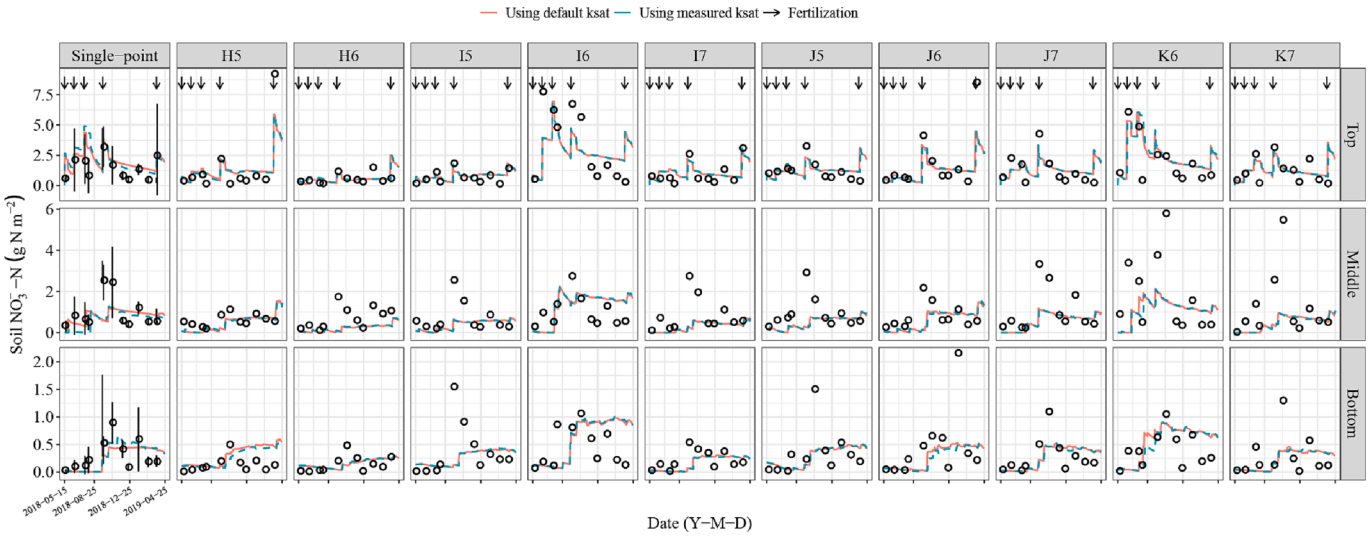

Fig. 8. Temporal comparison of measured (points) and simulated (lines) soil NO_3^--N content for the single-point simulation (scenarios 1 and 2 with default and measured k_{sat}, respectively) and grid-to-grid simulations (scenarios 3 and 4 with default and measured k_{sat}, respectively) at depths of 0–10 cm (Top), 10–20 cm (Middle), 20–30 cm (Bottom) from May 2018 to April 2019. The x-axes are the same for all the grids as the single-point. Scenarios with the default k_{sat} are given with a red unbroken line, while those with measured k_{sat} are given with a blue dashed line. Grid-to-grid simulations are given at each of the ten grid cells highlighted in Fig. 1 (labelled H5, H6, I5, I6, I7, J5, J6, J7, K6 and K7). Times of fertilization are also shown. (For interpretation of the references to colour in this figure legend, the reader is referred to the web version of this article.)

Table 3
Statistical indices for soil NO_3^--N content at soil depths of 0–10 (Top), 10–20 (Middle), 20–30 cm (Bottom) for the single-point and grid-to-grid simulation scenarios with default and measured k_{sat}.

Soil layer	Index	Single-point (n = 12)		Grid-to-grid (n = 120)	
		Scenario 1 default k_{sat}	Scenario 2 measured k_{sat}	Scenario 3 default k_{sat}	Scenario 4 measured k_{sat}
Top	RMSE	1.38	1.53	0.71	0.74
	EF	−0.23	−0.51	0.68	0.64
	CD	2.31	1.43	2.01	1.92
	r	0.26	0.22	0.84	0.81
	ME	−0.68	−0.78	−0.18	−0.19
	RE	−46.86	−53.51	−12.48	−13.29
Middle	RMSE	1.09	1.09	1.13	1.12
	EF	−0.06	−0.06	−0.14	−0.12
	CD	8.35	5.36	4.00	4.14
	r	0.14	0.32	0.29	0.31
	ME	0.19	0.39	0.43	0.43
	RE	20.28	41.14	44.49	45.40
Bottom	RMSE	1.13	1.13	1.20	1.21
	EF	0.10	0.10	−0.01	−0.03
	CD	3.20	2.62	2.05	1.99
	r	0.38	0.39	0.34	0.33
	ME	0.04	0.01	0.00	0.01
	RE	12.47	4.34	1.40	2.95

Note: RMSE: the root mean squared error; EF: modelling efficiency; CD: the coefficient of determination; *r*: the correlation coefficient; RE: the relative error and ME: the mean error.

grazed evenly in the study field and their excreta were assumed similarly uniform and that fertiliser/manure was uniformly applied. This uniformity is unlikely to be the case, and in turn, the measurements of soil N could be compromised by a likely spatial unevenness in grazing or fertiliser/manure application.

The model also over-predicted NH_4^+-N and under-predicted NO_3^--N content in the lower soil layers (Figs. 6 and 8), where inherent complexities in the processes of N cycling and the connectivity between linked grid cells would be influential. Errors in the model estimation of nitrification/denitrification, organic matter decomposition, plant uptake and movement with water could exaggerate poor soil N simulations. The chosen interlinks among the grid cells based on the water potential moving direction could be too simplistic to reflect the actual water moving direction. Here, little change in the measured soil NH_4^+-N and NO_3^--N contents along the downstream water flux direction lines (Figs. 5 and 7) suggested an over-simplicity.

Model performance should be taken in context of inherent complexities, where an agroecological system at the within field level is multiscale in nature, characterized by strong heterogeneities and geometrical complexity. The grid-to-grid setting, as a kind of the asymptotic homogenization, should be able to exploit the sharp length scale separation that exits in such multiscale systems. As a power series representation of the field, the grid-to-grid setting can provide macroscale systems of partial differential equations, where derived models encode the role of the microstructure in their coefficients (hydraulic conductivities, diffusivities, elastic stiffness, etc.) (Penta and Gerisch, 2017).

4.4. Limitations and implications

4.4.1. Limitations

In summary, we can identify the following (linked) limitations to our simulation results: (a) the (arbitrary) determination of the grid sizes, (b) the highly localised nature of k_{sat} and (c) the assumption of the exchange of water and soil N between grids. We hypothesized that measuring k_{sat} at a spatial resolution of a 50 × 50 m grid would be acceptable for determining spatial patterns of soil water and mineral N content. However, measured k_{sat} displayed a highly localised nature – meaning the chosen resolution was likely too coarse. Previous studies have suggested that the complex water exchanges generally exhibit substantial spatial variability in the soil hydraulic properties (Jaffri et al., 2019; Schaap et al., 2001). Therefore, accuracy in simulating the spatial distribution of soil water and mineral N can be hampered by the measurement resolution of k_{sat}. With the grid-to-grid setting, we assumed that soil water and mineral N fluxes in a layer from a grid are added to the pools in the same layer of its adjacent lower grid. Further, vertical and lateral fluxes in a soil layer could be affected by grid resolution, field steepness, and the thickness of the soil layer. Further research is needed to investigate the implications of these factors for downward and lateral water and N movement at the field scale.

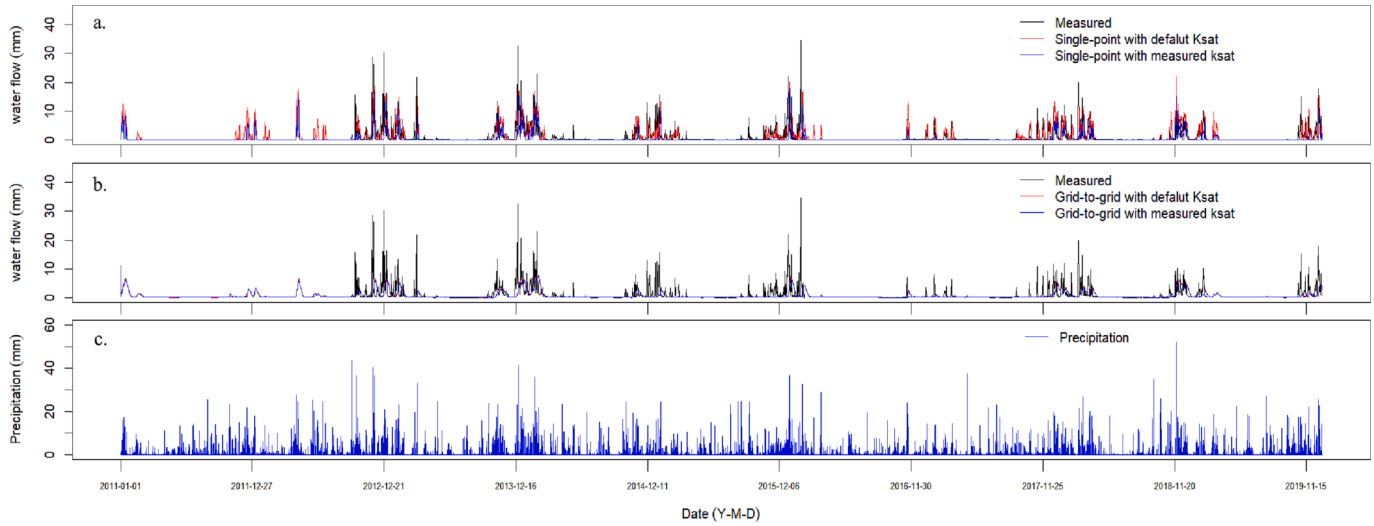

Fig. 9. Comparison of measured and simulated water fluxes from 2011 to 2019 for: (a) single-point (scenarios 1 and 2) and (b) grid-to-grid simulations (scenarios 3 and 4) between default and measured k_{sat}. Precipitation data are given for context (c).

Table 4
Statistical performance indices for water fluxes ($n = 2126$) for the single-point and grid-to-grid simulations at the sub-catchment scale, for the four scenarios.

Index	Single-point		Grid-to-grid	
	Scenario 1 default k_{sat}	Scenario 2 measured k_{sat}	Scenario 3 default k_{sat}	Scenario 4 measured k_{sat}
RMSE	1.99	1.85	2.13	2.16
EF	0.37	0.46	0.28	0.26
CD	1.05	2.48	5.28	5.76
r	0.68	0.72	0.59	0.57
ME	−0.13	0.65	0.60	0.61
RE	−11.58	56.13	51.80	52.33

Note: RMSE: the root mean squared error; EF: modelling efficiency; CD: the coefficient of determination; *r*: the correlation coefficient; RE: the relative error and ME: the mean error.

4.4.2. Implications

Our results have demonstrated that modified process-based models that are applied at the field scale can simulate the spatial dynamics of soil water and N content at a sub-field scale. In arable and grassland settings, soil hydraulic properties and agronomic inputs (e.g., fertilisers) are not always evenly distributed in a field. Thus, using simple field-scale averages of these variables in a (single-point) simulation can generate inaccurate simulations. If a field can be divided into cells, each of which has common properties and inputs, the aggregation of simulated outputs from individual cells (grid-to-grid simulation) can more accurately represent the outputs from the entire field. In this context, our results have implication for precision agriculture, which can recommend inputs at the right place and at the right time based on local environmental conditions and plant growth status. The modified model could also be extended to any scale, moving beyond the field to the farm, and above. For example, at the farm scale, each farm field with its own characteristics in soil properties and management practices can be treated as a cell. All fields of the farm can be connected by exchanging water and nutrients, enabling farm-level forecasts for water and nutrient budgets. Finally, the modified model could be usefully implemented within a digital twin of an agricultural system (Pylianidis et al., 2021), at a given scale (field, farm and above), dynamically updated by in situ or remotely sensed data.

5. Conclusions

This study investigated if key nutrient cycling components could be simulated more accurately than that found using defaults of the SPACSYS model, by considering within-field measurements of k_{sat}, together with a model specification that captures within-field water pathways. Using measured rather than estimated default values of k_{sat} was found to be of marginal value, where measured k_{sat} was only worthwhile for improving water flux simulation accuracy. For soil moisture and water flux simulations, the default field level setting was either sufficient or appropriate, respectively. For soil N simulations, the within-field setting was appropriate. Given the highly localised and skewed nature of the measured k_{sat}, it is unclear whether further work, with measured k_{sat} at some finer spatial resolution would revise (improve accuracy) or collaborate this study's findings. The former could indicate value in directing resources to measure k_{sat} for improving model performance, while the latter would not.

Declaration of Competing Interest

The authors declare that they have no known competing financial interests or personal relationships that could have appeared to influence the work reported in this paper.

Data availability

The link to download the data has been shared in acknowledgements

Acknowledgements

This work was supported by the Biotechnology and Biological Sciences Research Council (BBS/E/C/000I0320 and BBS/E/C/000I0330) and the Natural Environment Research Council Newton Fund (NE/N007433/1). CL, SY and QW received their studentships from the Chinese Scholarship Council. Authors also thank Charlie Morten and John Hunt for their help taking soil samples. The North Wyke Farm Platform is a UK National Capability, also supported by the Biotechnology and Biological Sciences Research Council (BBS/E/C/000J0100). All study data can be downloaded from the platform's data portal (http://resources.rothamsted.ac.uk/farmplatform).

Appendix A. Supplementary material

Supplementary data to this article can be found online at https://doi.org/10.1016/j.catena.2023.107058.

References

Alletto, L., Coquet, Y., 2009. Temporal and spatial variability of soil bulk density and near-saturated hydraulic conductivity under two contrasted tillage management systems. Geoderma 152, 85–94. https://doi.org/10.1016/j.geoderma.2009.05.023.

Baiamonte, G., Bagarello, V., D'Asaro, F., Palmeri, V., 2017. Factors influencing point measurement of near-surface saturated soil hydraulic conductivity in a small Sicilian basin. Land Degrad. Dev. 28, 970–982. https://doi.org/10.1002/ldr.2674.

Beskow, S., Timm, L.C., Tavares, V.E.Q., Caldeira, T.L., Aquino, L.S., 2016. Potential of the LASH model for water resources management in data-scarce basins: a case study of the Fragata River basin, southern Brazil. Hydrol. Sci. J. 61, 2567–2578. https://doi.org/10.1080/02626667.2015.1133912.

Bingham, I.J., Wu, L., 2011. Simulation of wheat growth using the 3D root architecture model SPACSYS: Validation and sensitivity analysis. Eur. J. Agron. 34, 181–189. https://doi.org/10.1016/j.eja.2011.01.003.

Centeno, L.N., Timm, L.C., Reichardt, K., Beskow, S., Caldeira, T.L., de Oliveira, L.M., Wendroth, O., 2020. Identifying regionalized co-variate driving factors to assess spatial distributions of saturated soil hydraulic conductivity using multivariate and state-space analyses. Catena 191, 104583. https://doi.org/10.1016/j.catena.2020.104583.

Cosby, B.J., Hornberger, G.M., Clapp, R.B., Ginn, T.R., 1984. A statistical exploration of the relationships of soil moisture characteristics to the physical properties of soils. Water Resour. Res. 20, 682–690. https://doi.org/10.1029/WR020i006p00682.

Dou, X., Wang, R., Zhou, X., Gao, F., Yu, Y., Li, C., Zheng, C., 2022. Soil water, nutrient distribution and use efficiencies under different water and fertilizer coupling in an apple–maize alley cropping system in the Loess Plateau, China. Soil Tillage Res. 218, 105308 https://doi.org/10.1016/j.still.2021.105308.

Harrod, T., Hogan, D., 2008. The soils of North Wyke and rowden. North Wyke Research, North Wyke, Devon.

Herbst, M., Pohlig, P., Graf, A., Weihermüller, L., Schmidt, M., Vanderborght, J., Vereecken, H., 2021. Quantification of water stress induced within-field variability of carbon dioxide fluxes in a sugar beet stand. Agric. For. Meteorol. 297, 108242 https://doi.org/10.1016/j.agrformet.2020.108242.

Jaffri, S.B., Nosheen, A., Iftikhar, S., Ahmad, K.S., 2019. Pedospheric environmental forensics aspects. In: Iftikhar, S. (Ed.), Trends of Environmental Forensics in Pakistan. Academic Press, pp. 39–59. Chapter 3.

Kreiselmeier, J., Chandrasekhar, P., Weninger, T., Schwen, A., Julich, S., Feger, K.-H., Schwärzel, K., 2020. Temporal variations of the hydraulic conductivity characteristic under conventional and conservation tillage. Geoderma 362, 114127. https://doi.org/10.1016/j.geoderma.2019.114127.

Li, Y., Liu, Y., Harris, P., Sint, H., Murray, P.J., Lee, M.R.F., Wu, L., 2017. Assessment of soil water, carbon and nitrogen cycling in reseeded grassland on the North Wyke Farm Platform using a process-based model. Sci. Total Environ. 603–604, 27–37. https://doi.org/10.1016/j.scitotenv.2017.06.012.

Lim, H., Yang, H., Chun, K.W., Choi, H.T., 2020. Development of pedo-transfer functions for the saturated hydraulic conductivity of forest soil in south korea considering forest stand and site characteristics. Water 12, 2217. https://doi.org/10.3390/w12082217.

Liu, Y., Li, Y., Harris, P., Cardenas, L.M., Dunn, R.M., Sint, H., Murray, P.J., Lee, M.R.F., Wu, L., 2018. Modelling field scale spatial variation in water run-off, soil moisture, N_2O emissions and herbage biomass of a grazed pasture using the SPACSYS model. Geoderma 315, 49–58. https://doi.org/10.1016/j.geoderma.2017.11.029.

Liu, C., Wang, L., Cocq, K.L., Chang, C., Li, Z., Chen, F., Liu, Y., Wu, L., 2020. Climate change and environmental impacts on and adaptation strategies for production in wheat-rice rotations in southern China. Agric. For. Meteorol. 292–293, 108136 https://doi.org/10.1016/j.agrformet.2020.108136.

Logsdon, S.D., 2013. Root Effects on Soil Properties and Processes: Synthesis and Future Research Needs. In: Timlin, D., Ahuja, L.R. (Eds.), Enhancing Understanding and Quantification of Soil–Root Growth Interactions, pp. 173-196.

Ming, F., Chen, L., Li, D., Wei, X., 2020. Estimation of hydraulic conductivity of saturated frozen soil from the soil freezing characteristic curve. Sci. Total Environ. 698, 134132 https://doi.org/10.1016/j.scitotenv.2019.134132.

Mohanty, B.P., Skaggs, T.H., Famiglietti, J.S., 2000. Analysis and mapping of field-scale soil moisture variability using high-resolution, ground-based data during the Southern Great Plains 1997 (SGP97) Hydrology Experiment. Water Resour. Res. 36, 1023–1031. https://doi.org/10.1029/1999WR900360.

Nikodem, A., Kodešová, R., Fér, M., Klement, A., 2021. Using scaling factors for characterizing spatial and temporal variability of soil hydraulic properties of topsoils in areas heavily affected by soil erosion. J. Hydrol. 593, 125897 https://doi.org/10.1016/j.jhydrol.2020.125897.

Orr, R.J., Murray, P.J., Eyles, C.J., Blackwell, M.S.A., Cardenas, L.M., Collins, A.L., Dungait, J.A.J., Goulding, K.W.T., Griffith, B.A., Gurr, S.J., Harris, P., Hawkins, J.M.B., Misselbrook, T.H., Rawlings, C., Shepherd, A., Sint, H., Takahashi, T., Tozer, K.N., Whitmore, A.P., Wu, L., Lee, M.R.F., 2016. The North Wyke Farm Platform: effect of temperate grassland farming systems on soil moisture contents, runoff and associated water quality dynamics. Eur. J. Soil Sci. 67, 374–385. https://doi.org/10.1111/ejss.12350.

Papanicolaou, A.N., Elhakeem, M., Wilson, C.G., Lee Burras, C., West, L.T., Lin, H., Clark, B., Oneal, B.E., 2015. Spatial variability of saturated hydraulic conductivity at the hillslope scale: Understanding the role of land management and erosional effect. Geoderma 243–244, 58–68. https://doi.org/10.1016/j.geoderma.2014.12.010.

Penta, R., Gerisch, A., 2017. An introduction to asymptotic homogenization. In: Gerisch, A., Penta, R., Lang, J. (Eds.), Multiscale Models in Mechano and Tumor Biology. Springer, Chambridge, pp. 1–26.

Peukert, S., Griffith, B.A., Murray, P.J., Macleod, C.J.A., Brazier, R.E., 2016. Spatial variation in soil properties and diffuse losses between and within grassland fields with similar short-term management. Eur. J. Soil Sci. 67, 386–396. https://doi.org/10.1111/ejss.12351.

Pylianidis, C., Osinga, S., Athanasiadis, I.N., 2021. Introducing digital twins to agriculture. Computers Electron. Agric. 184, 105942 https://doi.org/10.1016/j.compag.2020.105942.

Rathjens, H., Oppelt, N., 2012. SWATgrid: An interface for setting up SWAT in a grid-based discretization scheme. Comput. Geosci. 45, 161–167. https://doi.org/10.1016/j.cageo.2011.11.004.

Rathjens, H., Oppelt, N., Bosch, D.D., Arnold, J.G., Volk, M., 2015. Development of a grid-based version of the SWAT landscape model. Hydrol. Process 29, 900–914. https://doi.org/10.1002/hyp.10197.

Rienzner, M., Gandolfi, C., 2014. Investigation of spatial and temporal variability of saturated soil hydraulic conductivity at the field-scale. Soil Tillage Res. 135, 28–40. https://doi.org/10.1016/j.still.2013.08.012.

Schaap, M.G., Leij, F.J., van Genuchten, M.T., 2001. rosetta: a computer program for estimating soil hydraulic parameters with hierarchical pedotransfer functions. J. Hydrol. 251, 163–176. https://doi.org/10.1016/S0022-1694(01)00466-8.

She, D., Chen, Q., Luis, C., Samuel, B., Hu, W., Tamara Leitzke, C., Luciana, M.O., 2017. Multi-scale correlations between soil hydraulic properties and associated factors along a Brazilian watershed transect. Geoderma 286, 15–24. https://doi.org/10.1016/j.geoderma.2016.10.017.

Smith, P., Smith, J., Powlson, D., McGill, W., Arah, J., Chertov, O., Coleman, K., Franko, U., Frolking, S., Jenkinson, D., 1997. A comparison of the performance of nine soil organic matter models using datasets from seven long-term experiments. Geoderma 81, 153–225. https://doi.org/10.1016/S0016-7061(97)00087-6.

Song, J.-H., Her, Y., Yu, X., Li, Y., Smyth, A., Martens-Habbena, W., 2022. Effect of information-driven irrigation scheduling on water use efficiency, nutrient leaching, greenhouse gas emission, and plant growth in South Florida. Agric. Ecosyst. Environ. 333, 107954 https://doi.org/10.1016/j.agee.2022.107954.

Stanley, S., Antoniou, V., Askquith-Ellis, A., Ball, L.A., Bennett, E.S., Blake, J.R., Boorman, D.B., Brooks, M., Clarke, M., Cooper, H.M., Cowan, N., Cumming, A., Evans, J.G., Farrand, P., Fry, M., Hitt, O.E., Lord, W.D., Morrison, R., Nash, G.V., Rylett, D., Scarlett, P.M., Swain, O.D., Szczykulska, M., Thornton, J.L., Trill, E.J., Warwick, A.C., Winterbourn, B., Daily and sub-daily hydrometeorological and soil data (2013-2019) [COSMOS-UK]. NERC Environmental Information Data Centre. 10.5285/b5c190e4-e35d-40ea-8fbe-598da03a1185.

West, T.O., Brandt, C.C., Baskaran, L.M., Hellwinckel, C.M., Mueller, R., Bernacchi, C.J., Bandaru, V., Yang, B., Wilson, B.S., Marland, G., Nelson, R.G., Ugarte, D.G.D.L.T., Post, W.M., 2010. Cropland carbon fluxes in the United States: increasing geospatial resolution of inventory-based carbon accounting. Ecol. Appl. 20, 1074–1086. https://doi.org/10.1890/08-2352.1.

Whitson, I.R., 2020. Hydropedology of depression-toe slope interaction across a soil unit boundary at the Boreal-Prairie interface. Catena 187, 104349. https://doi.org/10.1016/j.catena.2019.104349.

Wösten, J.H.M., Pachepsky, Y.A., Rawls, W.J., 2001. Pedotransfer functions: bridging the gap between available basic soil data and missing soil hydraulic characteristics. J. Hydrol. 251, 123–150. https://doi.org/10.1016/S0022-1694(01)00464-4.

Wu, L., 2019. SPACSYS (v6.00) - Technical manual. Rothamsted Research, North Wyke, UK http://www.rothamsted.ac.uk.

Wu, L, Blackwell, M, Dunham, S, Hernández-Allica, J, McGrath, S P, 2019. Simulation of phosphorus chemistry, uptake and utilisation by winter wheat. Plants 8 (10), 404. https://doi.org/10.3390/plants8100404.

Wu, L., McGechan, M., McRoberts, N., Baddeley, J., Watson, C., 2007. SPACSYS: integration of a 3D root architecture component to carbon, nitrogen and water cycling—model description. Ecol. Model. 200, 343–359. https://doi.org/10.1016/j.ecolmodel.2006.08.010.

Wu, L., Rees, R., Tarsitano, D., Zhang, X., Jones, S., Whitmore, A., 2015. Simulation of nitrous oxide emissions at field scale using the SPACSYS model. Sci. Total Environ. 530, 76–86. https://doi.org/10.1016/j.scitotenv.2015.05.064.

Wu, L., Zhang, X., Griffith, B.A., Misselbrook, T., 2016. Sustainable grassland systems: A modelling perspective based on the North Wyke Farm Platform. Eur. J. Soil Sci. 67, 397–408. https://doi.org/10.1111/ejss.12304.

Zhang, Y., Hou, J., Cao, Y., Gu, J., Huang, C., 2017. OpenMP parallelization of a gridded SWAT (SWATG). Comput. Geosci. 109, 228–237. https://doi.org/10.1016/j.cageo.2017.08.002.

Zhang, X., Sahajpal, R., Manowitz, D.H., Zhao, K., LeDuc, S.D., Xu, M., Xiong, W., Zhang, A., Izaurralde, R.C., Thomson, A.M., West, T.O., Post, W.M., 2014. Multi-scale geospatial agroecosystem modeling: a case study on the influence of soil data resolution on carbon budget estimates. Sci. Total Environ. 479–480, 138–150. https://doi.org/10.1016/j.scitotenv.2014.01.099.

Zhang, X., Izaurralde, R.C., Manowitz, D.H., Sahajpal, R., West, T.O., Thomson, A.M., Xu, M., Zhao, K., LeDuc, S.D., Williams, J.R., 2015. Regional scale cropland carbon budgets: Evaluating a geospatial agricultural modeling system using inventory data. Environ. Model. Softw. 63, 199–216. https://doi.org/10.1016/j.envsoft.2014.10.005.

Zhang, X., Xu, M., Sun, N., Xiong, W., Huang, S., Wu, L., 2016. Modelling and predicting crop yield, soil carbon and nitrogen stocks under climate change scenarios with fertiliser management in the North China Plain. Geoderma 265, 176–186. https://doi.org/10.1016/j.geoderma.2015.11.027.